Cavity-mediated coupling of phonons and magnons

Yong-Pan Gao,[1] Cong Cao,[2] Tie-Jun Wang,[1,*] Yong Zhang,[1] and Chuan Wang[1,†]

[1]*School of Science and the State Key Laboratory of Information Photonics and Optical Communications, Beijing University of Posts and Telecommunications, Beijing 100876, China*

[2]*School of Ethnic Minority Education, Beijing University of Posts and Telecommunications, Beijing 100876, China*

(Received 15 January 2017; published 10 August 2017)

Optomagnonics and optomechanics have various applications, ranging from tunable light sources to optical manipulation for quantum information science. We propose a hybrid system based on the interaction between a phonon and a magnon that can be tuned by an electromagnetic field based on the radiation pressure and magneto-optical effects. The self-energies of the magnon and phonon induced by the electromagnetic field and the influence of the thermal noise are studied. Moreover, the topological features of the hybrid system are illustrated considering the dynamical encircling with the exceptional points, and the chiral characteristics under these encirclements are found.

DOI: 10.1103/PhysRevA.96.023826

I. INTRODUCTION

Optomechanics [1–10] and optomagnonics [11–22] are both hybrid optical interactions that can be achieved with microresonator systems. Efficient and low-noise optomechanics has many applications in classical and quantum photonics such as squeezed light generation [23–27], mass and force sensing [28–31], and optical manipulation [32–36]. Moreover, optomechanics also provides us with a platform to study the basic tasks of quantum information processing [37–40]. On the other hand, a magnon is the quantized magnetization excitation in magnetic materials [41–43], and optomagnonics describes the interaction between a photon and a magnon through the magnetic dipole interaction. The achievement of coherent information processing based on optomagnonics has recently emerged [44–46]. Because of their long lifetime [46–48], magnons are a good candidate for information storage.

Based on the magneto-optical (MO) effect, magnons can be generated and probed using the optical pumping process [49,50]. Most recently, optical-magnetic interactions have been experimentally achieved with a magnetic insulator yttrium iron garnet (YIG) microsphere cavity in the c band [13]. In that experiment, the magnon-phonon coupling strength could reach a level of 100 kHz in the cavity with a quality factor (Q factor) of 10^6. The first description of the optomechanical effect can be traced back to 1619, when Kepler presented the concept of radiation pressure to explain the observation that the tail of a comet always points away from the Sun. With the development of microfabrication technology, various schemes based on microresonator optomechanical systems have been theoretically proposed and experimentally achieved with improved cavity quality factors at decreased scales [51–53]. Recently, a scheme that takes the electromagnetic freedom as a medium was presented, and the dark state [32], multimode action [54], and topological features [55,56] were studied. The most famous study of MO effects [57] is the Faraday effect [58,59], which has been utilized in discrete optical device applications [60,61]. In this application, the electromagnetic field can also mediate the interaction between the magnon and phonon fields.

In this paper, we consider a high-quality YIG microsphere cavity with both optomechanical and optomagnetic properties. Here, we assume that the electromagnetic field operates in the whispering-gallery mode (WGM), and the transverse-magnetic (TM) and transverse-electric (TE) modes have slight frequency detuning, as there is a slight difference in their effective refractive indices [62]. Given the independently tunable frequency, the TE and TM modes play different roles in our system. We find that the electromagnetic field can introduce the self-energy component into the magnon and phonon and even bridge the interaction between the phonon and the magnon. Additionally, the chiral topological characteristics are studied.

This article is structured as follows: In Sec. II, we give the linearized Hamiltonian and the coupling equations in the frequency domain. Based on these equations, we obtain the self-energy and the mediated interaction in Sec. III A. In Sec. III B, we describe a method to manipulate the thermal environment of the magnon and phonon. In Sec. IV A, the eigenenergies of the magnon-phonon hybrid system are given, and we find the Riemann-surface-style energy scheme under the input field mediation. To further study the topological features, we show the dynamic adiabatic evolution of this system in Sec. IV B.

II. SYSTEM HAMILTONIAN

As shown in Fig. 1, the system under consideration is a YIG microsphere cavity. With the YIG doping, the electromagnetic field interacts with the magnetic resonator, which provides the phonon-magnon interaction. The glass sphere has an intrinsic mechanical frequency, which indicates that the intracavity field can drive the phonon-photon interaction. In Fig. 1(b), we draw a simplified diagram of the structure of the system. In this figure, the TE and TM fields are indicated by red and blue arrows, respectively. The YIG material, which is mixed in the entire cavity, is equivalent to a magnet resonator located at the center of the cavity. The electromagnetic fields are mainly propagated at the boundary of the cavity. We use the blue arrows to show the vibrations of the entire cavity along

*wangtiejun@bupt.edu.cn
†wangchuan@bupt.edu.cn

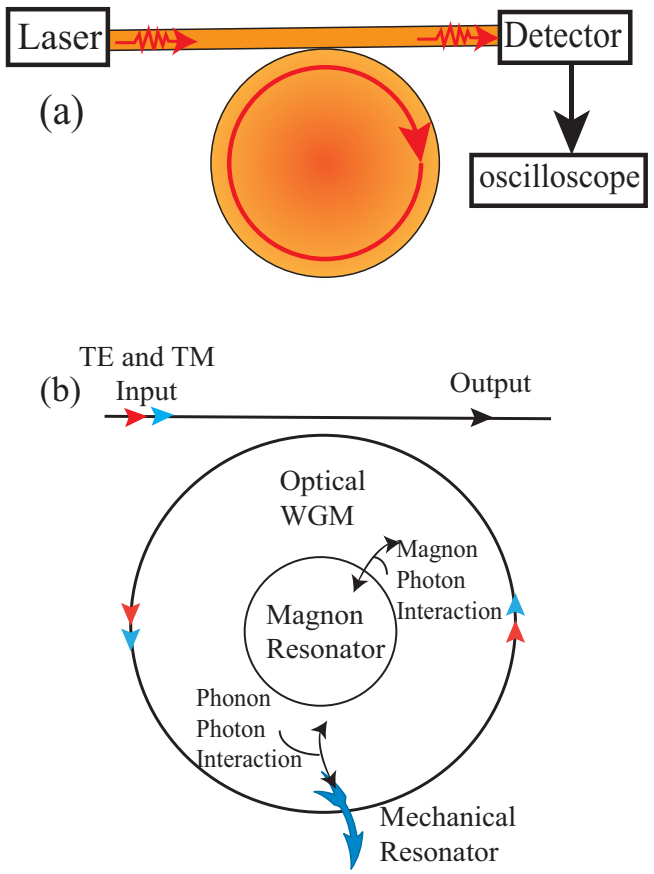

FIG. 1. The structure of the system studied in this article. (a) The objects of this system, a glass ball, and YIG in the mechanical mode. A fiber taper is coupled to the pumped field with the magnon-photon-phonon system. (b) The interaction scheme. The magnon and phonon systems were bridged through the phonon-photon and magnon-photon interactions. The red and blue arrows represent the TE and TM pumping, respectively.

the radial. The black double arrows indicate the presence of interaction. There is no interaction between the phonon and the magnon. This is because the nature of the magnon is determined by the nature of the miscellaneous material [11]. The weak vibration of the cavity does not change the properties of the material. So the interaction does not exist.

We use the nondepletion approximation [13] to eliminate the influence of TM field and eliminate the steady-state part of the TE field based on the perturbation method [33]. The effective Hamiltonian of the main part of the TE field dynamics is obtained as follows (a detailed deduction can be found in Appendix A):

$$H = \omega_b \hat{b}^\dagger \hat{b} + \omega_m \hat{m}^\dagger \hat{m} + \omega_r \hat{r}^\dagger \hat{r} + G_a \hat{b}^\dagger \hat{m} + G_a^* \hat{b} \hat{m}^\dagger + G_b (\hat{b}^\dagger + \hat{b}) \hat{z}, \quad (1)$$

where $G_a = g_m \langle a \rangle = g_m \sqrt{2\kappa_{a,1}} a_{in} / [-i(\omega_L - \omega_a) + \kappa_a]$ is the effective magnon-photon coupling strength, $G_b = g_b \langle b \rangle = g_b \sqrt{2\kappa_{b,1}} b_{in} / [-i(\omega_{pu} - \omega_b) + \kappa_b]$ is the effective phonon-photon coupling strength, ω_a (ω_b) is the frequency of the TM (TE) mode, ω_m is the magnetic frequency, and ω_r is the frequency of the phonon. $j^\dagger$ (j; with $j = a,b,m,r$) is the creation (annihilation) operator of the related mode (TM mode photon, TE mode photon, magnon, and phonon). g_m describes the interaction strength between the photon and the magnon, and g_b describes the interaction strength between the photon and the phonon. $\hat{z} = \hat{r}^\dagger + \hat{r}$ is the displacement operator of the phonon. Based on the Hamiltonian, we assume that the system's magneto-optical coupling and the mechanical-optical coupling are linearized by the strong input field. Under the perturbation approximation, we can obtain the coupling equations of the perturbation part in the frequency domain as (see Appendix B)

$$\chi_b^{-1}[\omega] b[\omega] = -i G_b z[\omega] - i G_a m[\omega], \quad (2a)$$

$$\chi_r^{-1}[\omega] r[\omega] = -i(G_b^* b[\omega] + G_b b^*[-\omega]) + \sqrt{\gamma_r}\eta_r[\omega], \quad (2b)$$

$$\chi_m^{-1}[\omega] m[\omega] = -i G_a b[\omega] + \sqrt{\gamma_m}\eta_m[\omega]. \quad (2c)$$

Here, $\chi_j[\omega] = [\gamma/2 - i(\omega - \omega_j)], j = b,r,m$, is the intrinsic susceptibility of its corresponding degree of freedom. γ_m and γ_r are the dissipations of phonons and magnons for the bath environment, respectively. $\eta_r[\omega]$ and $\eta_m[\omega]$ are the spectra of the bath environment of their corresponding degrees of freedom.

III. THE OPTICAL MODULATION OF THE PHONON-MAGNON INTERACTION

A. The mediated self-energy and interaction strength

The case of an optically mediated mechanical resonator has been studied in previous research [32]. To investigate the self-energy of the magnon and the mediating interaction, we eliminate the electromagnetic part $b[\omega]$ of the system and solve the self-energy part of the system. In addition, we neglect the effective interaction terms between the phonon and the magnon:

$$\left(\chi_m^{-1}[\omega] + i\Sigma_{mm}[\omega]\right) m[\omega] = \sqrt{\gamma_m}\eta_m[\omega], \quad (3a)$$

$$\left(\chi_r^{-1}[\omega] + i\Sigma_{rr}[\omega]\right) z[\omega] = \sqrt{\gamma_r}\eta_r[\omega], \quad (3b)$$

where $\Sigma_{rr}[\omega] = -i|G_b|^2(\chi_b[\omega] - \chi_b^*[-\omega])$ denotes the optomechanical self-energy. Similarly, $\Sigma_{mm}[\omega] = -iG_a^2\chi_b[\omega]$ is defined as the self-energy of the magnon. This self-energy represents the contribution of the optomagnonics to the magnonic resonance frequency $\delta\omega_i = \mathrm{Re}(\Sigma_{mm}[\omega_i])$ and damping $\delta\gamma_i = \mathrm{Im}(\Sigma_{mm}[\omega_i]), i = m,r$. Here, G_a is mediated by the TM pumping field, and χ_c can be controlled by the detuning Δ_r of the TE optical pump field.

To study the relationship between the frequency detuning and self-energy, we assume that the TE mode is pumped with the frequency $\omega_L = \omega_b$ and the magnon is resonant with the phonon ($\omega_r = \omega_m$). For simplicity, we set $\gamma_m = \gamma_r = \kappa_a = \kappa_b = \gamma$. Suppose that both the TE and TM modes satisfy the critical coupling condition $\kappa_{i,1} = \kappa_i/2 (i = a,b)$ with the pumping field. Moreover, we take $a_{in} g_m = b_{in} g_b$ to ensure that G_a is comparable to G_b. Here, we set $\omega_r = 0.4\gamma$; then, the mechanical mode is operating in the unresolved-sideband regime. To intuitively show the influence of the pump field

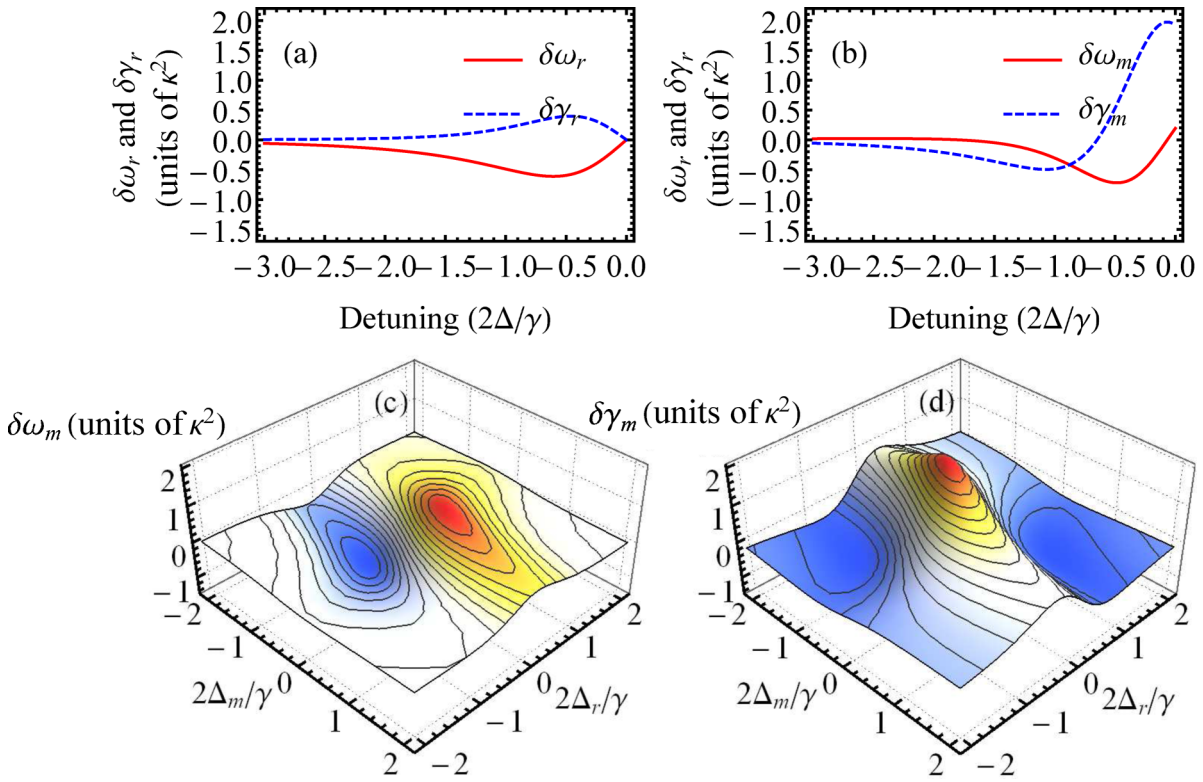

FIG. 2. The strength of the self-energy as a function of the detuning. In (a) and (b), we plot the frequency and the damping shift under different amounts of monochromatic driving, while in (c) and (d), we plot the frequency and the damping shift of the magnon, respectively, when the system is driven with different frequencies in the TM and TE modes. Here, the detuning-$\Delta = \Delta_m = \Delta r$ is plotted with the decay step γ. The amplitude of the frequency and the damping shift have units of $(g_i a_i \kappa)^2$. Here, (a) shows the frequency and damping shift of the mechanical resonator. The red solid line corresponds to the frequency shift, while the blue dashed line shows the damping modulation. (b) shows the same characteristics of the magnon.

frequency on the self-energy, we plot the mediated frequency and damping in Fig. 2. Here, $\Delta_r = \omega_{pu} - \omega_b, \omega_{pu}$ is the pumping frequency of the TE mode, $\Delta_m = \omega_L - \omega_a, \omega_L$ is the pumping frequency of the TE mode, and $\Delta = \Delta_r = \Delta_r$ shows the mode-detuning synchronous change. Compared with the self-energy of the mechanical resonator shown in Fig. 2(a) [32], the self-energy of the magnon is different. In Fig. 2(b), we plot the monochromatic pumped condition (the TM pump frequency is equal to the TE pump frequency). Figure 2(b) shows the difference in the self-energy between the magnon and the mechanical resonator, where both the mediated frequency and the damping of the magnon can be positive or negative valued. In general, positive and negative frequency detunings correspond to blueshifting and redshifting of the resonator, while for the damping term, positive and negative mean that the resonator is operating in the gain region and dissipative region, respectively. Thus, shifting and damping features are tunable for the magnon but not for the mechanical resonator. To further study the characteristics of the self-energy of the magnon, we plot a three-dimensional graph to show the influence of the frequency of the TE and TM fields. Figure 2(c) shows the frequency shift of the magnon, while in Fig. 2(d), we show the dissipation's variation under different TE and TM pump detunings. As shown in these two plots, the action of the frequency shift and the damping changes are not synchronized. In this sense, we can independently control the frequency and damping.

The self-energy term shows the interaction between the resonators and the optical field, while the interaction term represents the interface between the magnon and the phonon. To study its influence, we rewrite Eq. (3) considering the mediated interaction

$$\left(\chi_m^{-1}[\omega] + i\,\Sigma_{mm}[\omega]\right)m[\omega] = \sqrt{\gamma_m}\eta_m[\omega] - i\,\Sigma_{mr}[\omega]z[\omega], \tag{4a}$$

$$\left(\chi_r^{-1}[\omega] + i\,\Sigma_{rr}[\omega]\right)z[\omega] = \sqrt{\gamma_r}\eta_r[\omega] - i\,\Sigma_{rm}[\omega]m[\omega] + i\,\Sigma_{rm}^*[-\omega]m^*[-\omega]. \tag{4b}$$

Here, $\Sigma_{mr}[\omega] = -iG_aG_b\chi_b[\omega]$ and $\Sigma_{rm}[\omega] = -iG_aG_b^*\chi_b[\omega]$ are the mediated interaction strengths. The coupling exhibits different coupling dissipations. Meanwhile, G_a and G_b can be mediated by the TE and TM pumping frequencies. Then, we can control the interaction strength by modulating the pump field. To simplify the results, we set $\omega_r = \omega_m$, $\gamma_m = \gamma_r = \kappa_a = \kappa_b = \gamma$, and $\kappa_{j,1} = \kappa_j/2$ $(j = a,b)$. In Fig. 3, we plot the strength and phase parts of the interaction strength of the mechanical resonator on the magnon and those of the magnon on the mechanical resonator. Figures 3(a) and 3(b) show the strength and phase of $\Sigma_{mr}[\omega_i]$, respectively, while the strength and phase of $\Sigma_{rm}[\omega_i]$ are exhibited in Figs. 3(c) and 3(d). Clearly, these two coupling strengths are equal. We know that the absolute phase of the interaction will not

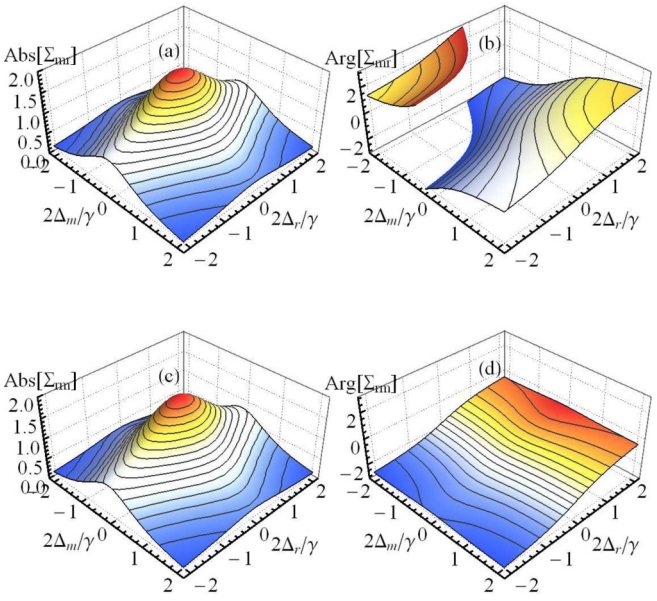

FIG. 3. The real and imaginary parts of the mediated coupling strength. We show Σ_{mr} in (a) and (b), while Σ_{rm} are shown in (c) and (d). Here, (a) and (c) represent the real part, while (b) and (d) show the imaginary part. Here, the detuning Δ is plotted with step decay γ. The amplitude of the frequency and the damping shift are in units of $(g_i a_i \kappa)^2$. The subscript ij indicates the effect of i on the j system.

influence the features of the system. However, as shown in Figs. 3(b) and 3(d), the coupling phase will be different in most regions of this system. Thus, there will be a relative phase. From Eq. (4), we can also find that there is a phase difference originating from the G_b and G_b^* terms. This relative phase gives us an additional degree of freedom to control the system. Moreover, the generation of this relative phase is a specific feature of this hybrid system.

B. The transverse electric field transmission

To further describe the magnon-phonon system using the electromagnetic field, we first give the expression of the electromagnetic field of the TE mode as

$$b[\omega] = \frac{X[\omega]Y[\omega]X^*[-\omega] + X[\omega]}{1 - X[\omega]Y[\omega]X^*[-\omega]Y^*[-\omega]} Z[\omega], \tag{5a}$$

$$X[\omega] = \left\{\chi_b^{-1}[\omega] + G_b^* G_b(\chi_r[\omega] - \chi_r^*[-\omega]) + G_a^2 \chi_m[\omega]\right\}^{-1}, \tag{5b}$$

$$Y[\omega] = G_b^2(\chi_r[\omega] - \chi_r^*[-\omega]), \tag{5c}$$

$$Z[\omega] = -iG_b(\chi_r[\omega] + \chi_r^*[-\omega])\sqrt{\gamma_r}\eta_r - iG_a\chi_m[\omega]\sqrt{\gamma_m}\eta_m. \tag{5d}$$

In these equations, the effective photon-magnon input term $Z[\omega]$ is affected by the environment of the magnetic and mechanical resonator, which is described by the expression of the electromagnetic field $b[\omega]$. Here, we take a thermal noise environment as an example to study the features of this system. The magnetic and mechanical modes of the resonator have quality factors $Q_r = Q_m \sim 1 \times 10^3$. Considering the stochastic and incoherent features, we assume that

$$S_Z[\omega] = \delta_{r,m} Z^*[\omega_1] Z[\omega]. \tag{6}$$

The thermal noise spectrum is $k_B T/\omega$, which could be set as a constant, as the change in the frequency ($|\omega_r - \omega_m|$) is negligible when compared with the frequency that we studied (ω_r, ω_m). The thermal noise is set as a unit value, as the effect of the noise exists throughout the system. Here, the terms $a_{in}g_m$ and $b_{in}g_r$ are chosen as a whole part. Considering that $a_{in}g_m \sim b_{in}g_r \sim 1$ THz, $g_m \sim 100$ Hz [13], $g_m \sim 1000$ Hz [63], and the wavelength is approximately 1550 nm, we can calculate that the TM mode pumping power $P_m \sim 20$ mW, while the TE pumping power is $P_r \sim 200$ μW. In addition, the damping rate of this system is set as $\kappa_a = \kappa_b = \kappa_m = \kappa_r = 20$ MHz. The magnon and photon have frequencies of $\omega_m = 1$ GHz $-$ 150 MHz and $\omega_r = 1$ GHz $+$ 150 MHz. It is worth noting that the parameters we set are experimentally achievable, except requiring the quality factor of the cavity to reach 10^7. To our knowledge, the quality factor of the magnetic cavity is experimentally 3×10^6 [13].

Because the intrinsic susceptibility of the system is sensitive to the frequency, the thermal noise will drive this system effectively under the resonance condition. In this structure, both the pump frequency and the pump power of the electromagnetic field as well as the TE and TM fields can be modulated. We further study the system using the optical spectrum under the influence of thermal noise in Fig. 4. In Fig. 4(a), we plot the effective pumping $a_{in}g_m = b_{in}g_r = 0.6$ THz, and we set the detuning of the TM pumping field to zero ($\Delta_m = \omega_L - \omega_a = 0$, where ω_L is the pumping frequency of the TM field). The thermal noise can be observed in the frequency domain of the TE mode. In Fig. 4(a), the maximal value of the electromagnetic field corresponds to the condition in which the thermal noise is resonant with the phonon-magnon system; then, the effective frequency of the phonon-magnon hybrid resonator can be read out. In Fig. 4(d), we show the influence of the TM detuning on the spectrum.

By increasing the pumping power, the optically mediated effect becomes obvious. The electromagnetic field operates as an optical spring under this condition and connects the phonon and magnon system by producing an effective coupling between them. To discuss this strong pumping region, we enlarge this effective driving strength to $a_{in}g_m = b_{in}g_r = 3.6 \times 10^{12}$ Hz. Figures 4(b) and 4(c) show the influence of the TE pump detuning. In Fig. 4(b), the TM detuning is set as $\Delta_m = 0$ Hz, whereas it is $\Delta_m = -3$ MHz in Fig. 4(c). Three bands can be observed in this system: the magnon band, the phonon band, and the optical spring band. The left band corresponds to the magnon mode, and there is an obvious frequency shift in the magnon mode. The magnon mode disappears when the detuning is larger than -10 MHz. This means that the magnon mode becomes a dark mode. The interaction between the magnon mode and the optical field disappears when it interferes with the optical and mechanical

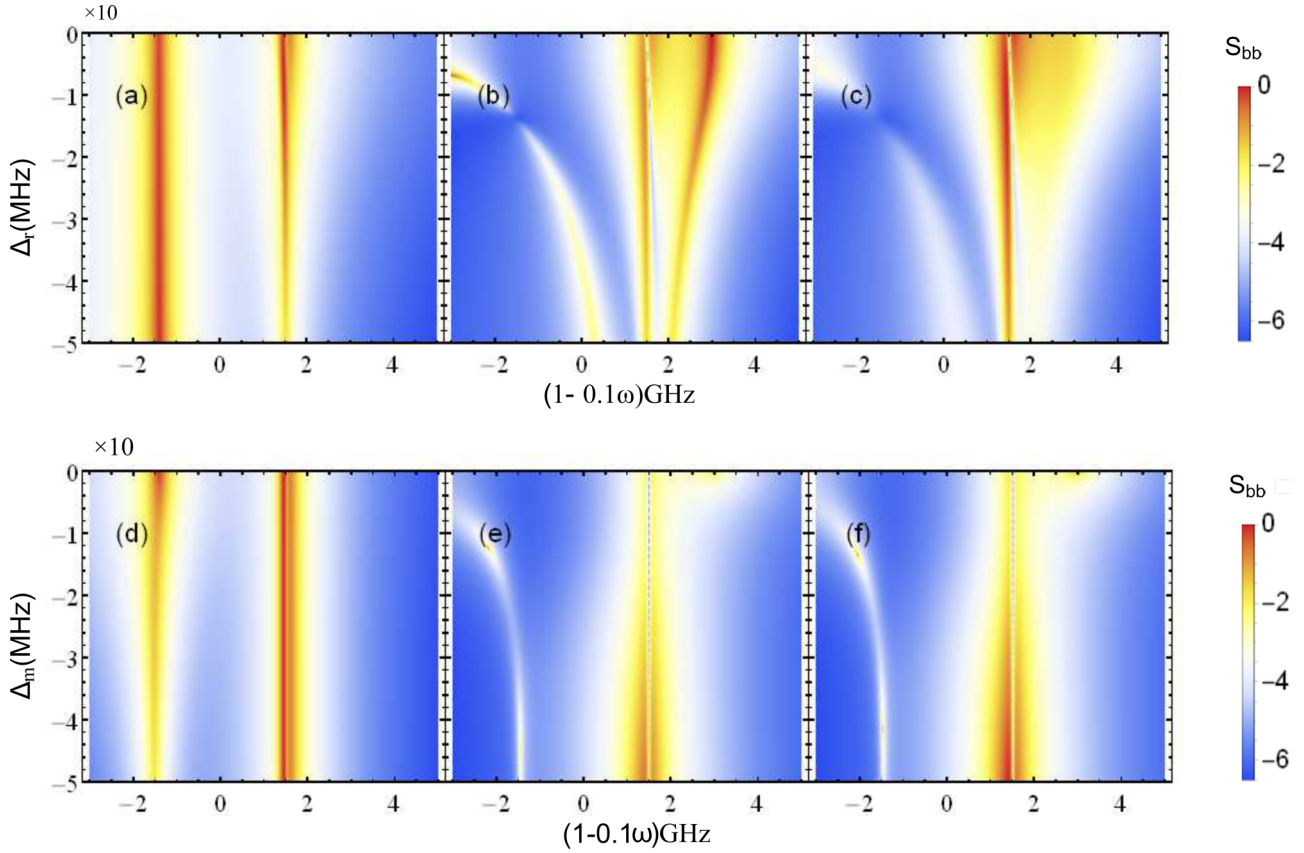

FIG. 4. Power spectral density (arbitrary units) of the heterodyne signal. (a), (b), and (c) TE and (d), (e), and (f) TM as a function of the measurement frequency (horizontal axis) and the detuning between the incident laser and the cavity resonance (vertical axis). The data in (a) and (d) show that the low effective input power $a_{in}g_m = b_{in}g_r = 0.6$ THz. This power is $a_{in}g_m = b_{in}g_r = 3.6$ THz in (b), (c), (e), and (f). In (a) and (b), the TM detuning is set as $\Delta_m = 0$ Hz, while in (c), $\Delta_m = -3$ MHz. In (d) and (e), the TE detuning is set as $\Delta_m = 0$ Hz, while in (f), $\Delta_m = -3$ MHz.

hybrid interaction. In Fig. 4(c), we see that the third band obviously changes under a slight detuning of the TM mode. We can conclude that the band on the right is associated with the optical spring effect.

The influence of the TM detuning is shown in Figs. 4(e) and 4(f). We see that only the third band can be found in the zero-detuning region. In these two plots, the magnon mode is weaker than the phonon mode, and it comes from the relative coupling phase of the magnon-photon to the phonon-photon. In addition, we see in both Figs. 4(e) and 4(f) that the dark magnon state appears when the pumping detuning is larger than -10 MHz. In addition, when the TM detuning is sufficiently large, the effective frequency shift is not as obvious. This can be explained as follows: When the detuning is strong, the magnon is decoupled from this system. Then, the magnon mode cannot be found in the optical field. In contrast to Fig. 4(e) with $\Delta_r = \omega_{pu} - \omega_b = 0$, where ω_{pu} is the pumping frequency of the TE mode, Fig. 4(f) is plotted under a detuning of $\Delta_r = -3$ MHz. We see that these two optical spectra are identical. The TE detuning influences only the absolute intensity of the field in the plotted region.

IV. THE TOPOLOGICAL FEATURES OF THE HYBRID PHONON-MAGNON SYSTEM

A. Topological energy with exceptional points

We consider a system that combines the magnon and phonon as a closed system, including optical pumping. For simplicity, we study the mechanical mode in the phonon mode but not the displacement momentum operator. The reduced Hamiltonian can be written as (a detailed derivation can be found in Appendix C)

$$H = \begin{Bmatrix} \omega_r - i\frac{\kappa_r}{2} & 0 \\ 0 & \omega_m - i\frac{\kappa_m}{2} \end{Bmatrix} - i \begin{Bmatrix} |G_b|^2[\chi_b[\omega_m] - \chi_b^*[-\omega_m] & G_a^* G_b \chi_b[\omega_m] \\ G_a G_b \chi_b[\omega_m] & G_a^2 \chi_b[\omega_m] \end{Bmatrix}. \quad (7)$$

Given the exact diagonalization of the Hamiltonian, two eigenenergies are found as a function of the pumping power and detuning of the TE field in Fig. 5. This system will include the exceptional points (EPs) if the system is tuned at $16|G_a|^2 G_b^2 \chi_b^2 + [2|G_b|^2(\chi_b^* - \chi_b) + 2G_a^2 G_b + \kappa_m - \kappa_r + 2i(\omega_m - \omega_r)]^2 = 0$. To satisfy the equality condition, both the

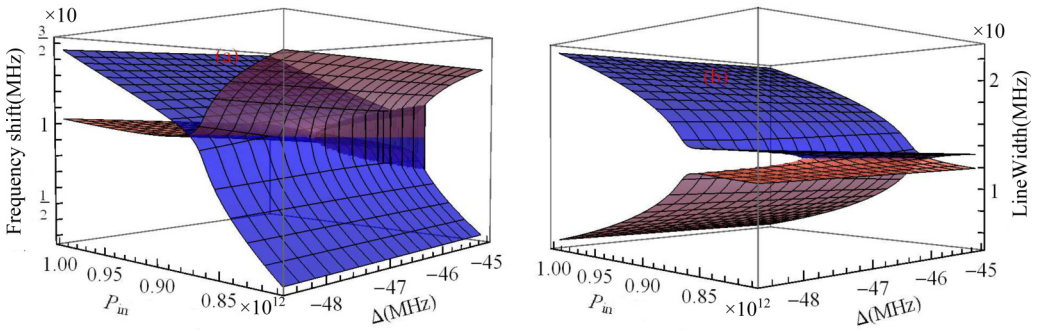

FIG. 5. The energy scheme of this hybrid system. (a) The real part and (b) the imaginary part. Here, $P_{in} = a_{in}g_m = b_{in}g_r$ is the effective input strength, while Δ is the frequency detuning of the TE mode. The TM mode detuning is set as -3 MHz. We use Δ to denote Δ_r, the TE detuning. Here, the cavity, magnon, and phonon dissipation is 20 MHz. The magnon has a frequency of 1 GHz $-$ 16 MHz, while the frequency is 1 GHz $+$ 16 MHz for the phonon.

real and imaginary parts should be controlled. Fortunately, G_a and G_b are both pumping frequency and strength dependent, and χ_b can also be controlled by the TE pumping frequency. To simplify this study, we set the TM detuning equal to the TE detuning; moreover, the effective pumping rates are set to be equal.

In Fig. 5, we show the real and imaginary parts of the eigenenergy of the mediated Hamiltonian in Eq. (7). In addition, we take the parameters shown in the previous section, except that the magnon frequency is 984 MHz, while the phonon has a frequency of 1016 MHz. Moreover, we fix the value of the TM detuning as $\Delta_a = -3$ MHz. The input field can be written in the effective form $P_{in} = a_{in}g_m = b_{in}g_r$. For the eigenfrequency, we plot its shift from 1 GHz. Here, the EPs are obvious. The two eigenenergy surfaces of the two supermodes form a Riemann surface; this gives the system a topological feature when the optical pumping encircles in different directions on the surface. As shown in Fig. 5(b), we find that the dissipation can be negative valued. This means that the optical field can operate as a gain medium, while the gain energy comes from the pumping field.

B. Topological encircling and state evolution

To further study the topological features of this system, we encircle this system in different directions on the Riemann surface. We make this system encircle along a closed path, and we study the differences when the EPs are included in and excluded from this circle. Taking Fig. 5 as a reference, we choose the encircling center point as $P_{in} = 0.87$ THz, $\Delta = -5.5$ MHz and $P_{in} = 0.87$ THz, $\Delta = -4.5$ MHz. Here, $P_{in} = a_{in}g_m = b_{in}g_r$ is the effective input power, while Δ denotes the frequency detuning of the TE mode. The TM mode detuning is set as -3 MHz. Here, we set the encircling radius as 1 unit, where 1 unit is 0.1 THz (1 MHz) on the P_{in} (Δ) axes. Considering the feature of the topological surface, we also need to encircle this system in different directions.

We plot the energy fraction of modes a and b of the studied system when encircling this system on the Riemann surface. Here, mode a corresponds to the red surface of this system, while mode b corresponds to the blue part. In Fig. 6, we always use the initial mode vectors to project the destiny matrix. In Figs. 6(a) and 6(b), we plot the mode evolution of the magnon-phonon supermode when the system is encircled in the direction shown. Additionally, the red line corresponds to mode a, while the blue line denotes mode b. Figures 6(c) and 6(d) include an additional phase π that makes the mode evolution synchronized with Fig. 6(b). Here, this system is encircling with a period of $T = 10$ ms to ensure that the adiabatic evolution of this system has a frequency on the order of gigahertz.

We analyze the phenomenon shown in Figs. 6(a) and 6(b). In these plots, the encircling region does not include the EP points. We can find the mode evolution in almost the same way. Given the adiabatic evolution, this system shows similar features when encircling in different directions. A tiny difference appears when the system remains on a different Riemann surface. In contrast to the above condition, when we include the EP points in the encircling, the evolution of this system will be quite different. As shown in Figs. 6(c) and 6(d), the difference is that the system will experience an acute oscillation even when this system evolves slowly. After the oscillation, there is a crossover between the two energy levels. This means that there is an energy-level variation occurring during the evolution. The EP points act as phase change points as the system experiences a sudden change in energy when encircling. Moreover, the system is different when it evolves in different directions. The main differences in the oscillation are the strength and lasting time. These differences can be attributed to the EP points with chirality when encircling, as shown in Fig. 5.

V. SUMMARY

In summary, we theoretically investigated an electromagnetic cavity-mediated phonon-magnon interaction system and elaborated on how to connect the phonon and magnon modes through optical mediation. As a medium, the electromagnetic field will produce a self-energy and mediate the interaction between the magnon and the phonon. When taking thermal noise as an example to study the influence of the environment, we found that the thermal field influences the output of the electromagnetic field. Moreover, the magnon will become a dark state when the detuning is small. Based on the coupling equations, we investigated the topological features of the hybrid system with the Hamiltonian. When encircling with the EPs on the Riemann energy surface, the energy-

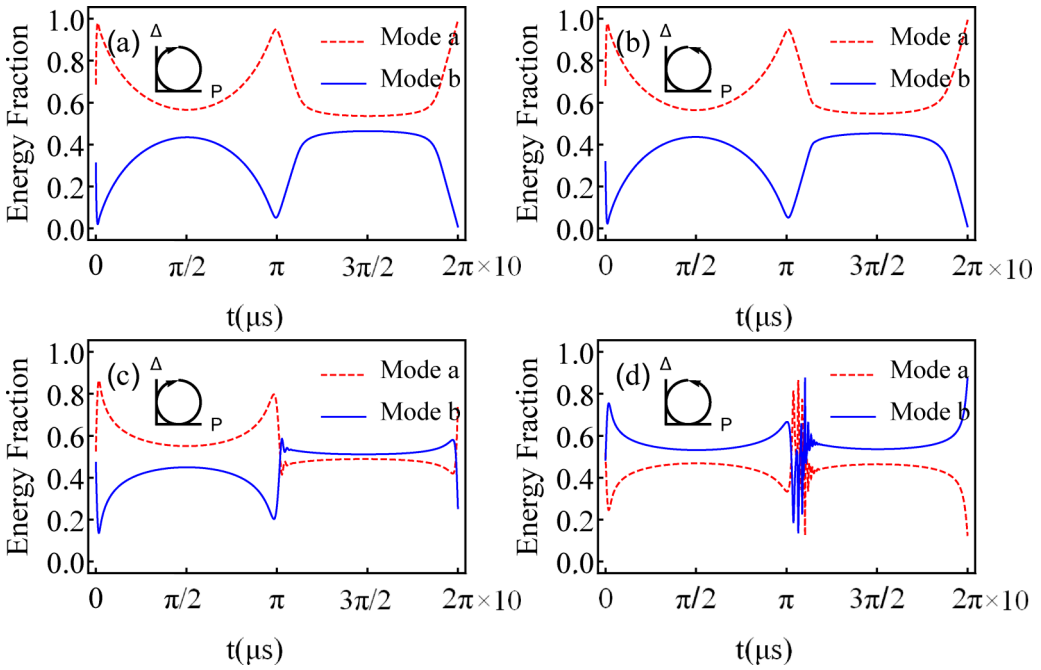

FIG. 6. Energy fraction under topological encircling. Here, the effective input power encircling center $P_{in} = a_{in}g_m = b_{in}g_r = 0.87$ THz. We use Δ to denote Δ_b, the TE detuning. Here, the encircling center on the Δ axes is $\Delta = -5.5$ MHz in (a) and (b), while it is -4.5 MHz in (c) and (d). (a) and (b) present encircling without EP points, while (c) and (d) include encircling under this setting. The TM mode detuning is set as -3 MHz. The encircling radius is 1 unit, and 1 unit is 0.1 THz on the P_{in} axes; on the Δ axes, it is 1 MHz. Here, the cavity, magnon, and phonon dissipations are 20 MHz. The magnon has a frequency of 1 GHz $-$ 16 MHz, while it is 1 GHz $+$ 16 MHz for the phonon. The encircling direction is as shown.

level projection presents different vibration behaviors, which indicate the chirality of the system.

ACKNOWLEDGMENTS

The authors gratefully acknowledge the support from the National Natural Science Foundation of China through Grants No. 61622103, No. 61471050, and No. 61671083; the Ministry of Science and Technology of the People's Republic of China (MOST) (2016YFA0301304); the Fok Ying-Tong Education Foundation for Young Teachers in the Higher Education Institutions of China (Grant No. 151063); and the Open Research Fund Program of the State Key Laboratory of Low-Dimensional Quantum Physics, Tsinghua University, Grant No. KF201610. Additionally, we would like to thank Dr. Q.-K. He for helpful discussions.

APPENDIX A: THE EFFECTIVE HAMILTONIAN OF THIS SYSTEM

We input signals that include both TE and TM modes, and we suppose that the coupling strength between the TM mode and the mechanical mode g_a is far less than that of the TE mode and mechanical mode g_b, i.e., $g_a \ll g_b$. In this sense, the Hamiltonian is [2,11]

$$H = \omega_a \hat{a}^\dagger \hat{a} + \omega_b \hat{b}^\dagger \hat{b} + \omega_m \hat{m}^\dagger \hat{m} + \omega_r \hat{r}^\dagger \hat{r} + g_m(\hat{a}\hat{b}^\dagger \hat{m} + \hat{a}^\dagger \hat{b}\hat{m}^\dagger) + g_b \hat{b}^\dagger \hat{b}(\hat{r}^\dagger + \hat{r}). \quad \text{(A1)}$$

Here, the Hamiltonian contains the free part, the magneto-optical interaction part [42], and the optical-mechanical interaction part [2], where ω_a (ω_b) is the frequency of the TM (TE) mode, ω_m is the magnetic frequency, and ω_r is the frequency of the phonon. $j^\dagger$ (j; with $j = a,b,m,r$) is the creation (annihilation) operator of the corresponding mode (TM mode photon, TE mode photon, magnon, and phonon). g_m is the interaction strength of the photon and magnon, and g_b is the interaction strength of the electromagnetic mode b and the phonon. The coupling between mode a and the mechanical mode is zero for the direction of the mechanical mode, and the field direction of mode a is orthogonal [2,64]. The TM mode is driven by $\sqrt{2\kappa_{a,1}}a_{in}(\hat{a}e^{i\omega_L t} + \hat{a}^\dagger e^{-i\omega_L t})$. $\kappa_{a,1}$ is the coupling damping between the fiber taper and the microcavity. $a_{in} = \sqrt{P_m/\hbar\omega_L}$ is the input strength of the TM mode, and ω_L is the TM pumping frequency. Because the TM field is used only to enhance the coupling strength between the TE field and the magnon, P_m is the driving power of the TM mode, and this TM mode is steady state under strong pumping. Then under the nondepletion approximation, the intracavity TM field is [13]

$$\langle a \rangle = \frac{\sqrt{2\kappa_{a,1}}a_{in}}{-i(\omega_L - \omega_a) + \kappa_a}, \quad \text{(A2)}$$

where κ_a is the total damping of the TM mode of the cavity. $\langle a \rangle$ corresponds to the interaction enhancement of the interaction between the TE photon and magnon modes. We write this effective coupling strength as $G_a = g_m\langle a \rangle$. Then under the nondepletion approximation [13], eliminating mode a, the

effective Hamiltonian can be written as

$$H = \omega_b \hat{b}^\dagger \hat{b} + \omega_m \hat{m}^\dagger \hat{m} + \omega_r \hat{r}^\dagger \hat{r} + G_a \hat{b}^\dagger \hat{m} + G_a^* \hat{b} \hat{m}^\dagger + g \hat{b}^\dagger \hat{b} (\hat{r}^\dagger + \hat{r}). \tag{A3}$$

For the cavity electromagnetic field, mode b is driven by the Hamiltonian as follows [33]:

$$H_{\mathrm{drive},b} = \sqrt{2\kappa_{b,1}} b_{in} (\hat{b} e^{i\omega_{pu} t} + \hat{b}^\dagger e^{-i\omega_{pu} t}). \tag{A4}$$

Here, $b_{in} = \sqrt{P_r/\hbar\omega_{pu}}$ is the driving strength of mode b. P_r is the driving power for the TE mode. ω_{pu} is the pumping frequency of the TE mode.

The Heisenberg equation of the Hamiltonian (A3) under the drive (A4) has the form

$$\dot{b} = -\left(\frac{\kappa}{2} - i\omega_b\right) b - i G_b z - i G_a m + \sqrt{2\kappa_{b,1}} b_{in} \exp(-i\omega_{pu} t), \tag{A5a}$$

$$\dot{r} = -\left(\frac{\gamma_r}{2} + i\omega_r\right) r - i g \hat{b}^\dagger \hat{b}, \tag{A5b}$$

$$\dot{m} = -\left(\frac{\gamma_m}{2} + i\omega_m\right) r - i G_a b. \tag{A5c}$$

The steady-state solution of the cavity strength b can be solved as

$$\bar{b} = \sqrt{2\kappa_{b,1}} b_{in} / [\kappa - i(\omega_{pu} - \omega_b) - g(\bar{r}^* + \bar{r})]. \tag{A6}$$

The term $-g(\bar{r}^* + \bar{r}, \bar{r} = \langle \hat{r} \rangle)$ is the displacement of the steady state of the mechanical resonators. We update $\omega_{b,\mathrm{new}} = \omega_b + g(\bar{r}^* + \bar{r})$. In the experiment, we only need to adjust the tunable laser to the resonant position; then we can achieve the above substitution steps. This approximation method can also be found in the supplementary material of Ref. [33]. It is worth noting, however, that the equilibrium position of the mechanical resonator is affected by both the electromagnetic field mode and the magnon modes. Based on perturbation approximation, i.e., $\hat{b} = \bar{b} + \hat{b}$, we can write the Hamiltonian of Eq. (A3) as

$$H = \omega_b (\bar{b} + \hat{b}^\dagger)(\bar{b} + \hat{b}) + \omega_m \hat{m}^\dagger \hat{m} + \omega_r \hat{r}^\dagger \hat{r} + G_a (\bar{b} + \hat{b}^\dagger) \hat{m} + G_a^* (\bar{b} + \hat{b}) \hat{m}^\dagger + g(\bar{b} + \hat{b}^\dagger)(\bar{b} + \hat{b})(\hat{r}^\dagger + \hat{r}). \tag{A7}$$

When omitting the term that shifts the mechanical resonator's equilibrium position and high-order perturbation, the effective Hamiltonian has the form

$$H = \omega_b \hat{b}^\dagger \hat{b} + \omega_m \hat{m}^\dagger \hat{m} + \omega_r \hat{r}^\dagger \hat{r} + G_a \hat{b}^\dagger \hat{m} + G_a^* \hat{b} \hat{m}^\dagger + G_b (\hat{b}^\dagger + \hat{b}) \hat{z}. \tag{A8}$$

Here, $\bar{b}$ is the steady-state solution of Eq. (A3) under the driving field (A4), and $\hat{z} = \hat{r}^\dagger + \hat{r}$. The effective coupling strength $G_b = \bar{b} g_b = \sqrt{2\kappa_{b,1}} b_{in} / [\kappa - i(\omega_{pu} - \omega_b)]$. In this Hamiltonian, $\hat{b}$ is the perturbation term of the TE field. We have kept the form of $\hat{b}$ in the text because the perturbation field we studied reflects the main characteristics of the system dynamics.

APPENDIX B: THE COUPLING STRENGTH IN THE FREQUENCY DOMAIN

As is well known, a room-temperature experiment is firmly in the classical regime $\hbar\omega_a \gg k_B T$; we thus use a classical analysis. We also disregard all noise in the optical drive, therein applying the rotating frame of $\hat{U} = \exp(-i\omega_{pu} \hat{b}^\dagger \hat{b})$, and we use $\Delta_r = \omega_{pu} - \omega_b$ for simplicity. Then, the kinetic equations of this system can be expressed as

$$\dot{b} = -\left(\frac{\kappa}{2} - i\Delta_b\right) b - i G_b z - i G_a m, \tag{B1a}$$

$$\dot{r} = -\left(\frac{\gamma_r}{2} + i\omega_r\right) r - i(G_b^* b + G_b b^*) + \sqrt{\gamma_r}\eta_r, \tag{B1b}$$

$$\dot{m} = -\left(\frac{\gamma_m}{2} + i\omega_m\right) m - i G_a b + \sqrt{\gamma_m}\eta_m. \tag{B1c}$$

The equation in the frequency domain can be derived with the Fourier transform $f[\omega] = \int_{-\infty}^{+\infty} f[t] \exp[-i\omega t]\, dt$. Here, the magnon and phonon are bathed in thermal fluctuations, and the thermal Langevin force $\eta_i(t)$ is described by $\langle \eta_i(t) \rangle = 0$ and $\langle \eta_j^*(t) \eta_i(t) \rangle = \delta_{ij} \delta t - t' k_B T / \hbar\omega_i$; then we can get

$$-i\omega b[\omega] = -\left(\frac{\kappa}{2} - i\Delta_b\right) b[\omega] - i G_b z[\omega] - i G_a m[\omega], \tag{B2a}$$

$$-i\omega r[\omega] = -\left(\frac{\gamma_r}{2} + i\omega_r\right) r[\omega] - i(G_b^* b[\omega] + G_b b^*[-\omega]) + \sqrt{\gamma_r}\eta_r[\omega], \tag{B2b}$$

$$\dot{m} = -\left(\frac{\gamma_m}{2} + i\omega_m\right) r[\omega] - i G_a b[\omega] + \sqrt{\gamma_m}\eta_m[\omega]. \tag{B2c}$$

For simplicity, we rewrite the system as

$$\chi_b^{-1}[\omega] b[\omega] = -i G_b z[\omega] - i G_a m[\omega], \tag{B3a}$$

$$\chi_r^{-1}[\omega] r[\omega] = -i(G_b^* b[\omega] + G_b b^*[-\omega]) + \sqrt{\gamma_r}\eta_r[\omega], \tag{B3b}$$

$$\chi_m^{-1}[\omega] m[\omega] = -i G_a b[\omega] + \sqrt{\gamma_m}\eta_m[\omega]. \tag{B3c}$$

Here, $\chi[\omega] = [\gamma/2 - i(\omega - \omega_j)], j = b, r, m$, is the intrinsic susceptibility of its corresponding degree of freedom. γ_m and γ_r are the dissipations of phonons and magnons for the bath environment, respectively. $\eta_r[\omega]$ and $\eta_m[\omega]$ are the spectra of the bath environment of their corresponding degrees of freedom.

APPENDIX C: THE REDUCED HAMILTONIAN

Through algebraic substitution, we eliminate the electromagnetic freedom. Equation (4) in the main text [Eq. (B3)] can be written as

$$\chi_r^{-1}[\omega] r[\omega] = -|G_b|^2 [\chi_b[\omega] - \chi_b^*[-\omega]] r[\omega] - G_a^* G_b \chi_b[\omega] m[\omega], \tag{C1a}$$

$$\chi_m^{-1}[\omega] m[\omega] = -G_a^2 \chi_b[\omega] r[\omega] - G_a G_b \chi_b[\omega] r[\omega]. \tag{C1b}$$

As a closed system, we discard the thermal noise term. This can also be achieved by placing this system into a low-temperature environment. In this two-mode system, we define the self-energy as

$$\Sigma[\omega] = -i \begin{Bmatrix} |G_b|^2[\chi_b[\omega] - \chi_b^*[-\omega]] & G_a^* G_b \chi_b[\omega] \\ G_a G_b \chi_b[\omega] & G_a^2 \chi_b[\omega] \end{Bmatrix}. \quad \text{(C2)}$$

When combining the phonon and magnon as a whole vector $\mathbf{s}(t) = (r(t), m(t))^T$, Eq. (C1) can be written in the following matrix form:

$$-i\omega \mathbf{s}[\omega] = -\begin{Bmatrix} \frac{\kappa_r}{2} + i\omega_r & 0 \\ 0 & \frac{\kappa_m}{2} + i\omega_m \end{Bmatrix} \mathbf{s}[\omega] - i\Sigma[\omega]\mathbf{s}[\omega]. \quad \text{(C3)}$$

Note that $\Sigma[\omega]$ varies on the scale of γ, whereas these vector modes are susceptible to being driven only if they are substantially smaller than γ. Therefore, it is sufficient to consider $\Sigma[\omega] \approx \Sigma[\omega_r] \approx \Sigma[\omega_m] \equiv \Sigma$ [55]. Then, the self-energy is frequency independent. Therefore, we can easily transform back into the time domain to obtain the effective Schrödinger's equation:

$$i\dot{\mathbf{s}}(t) = H\mathbf{s}(t). \quad \text{(C4)}$$

Here, the Hamiltonian reads

$$H = \begin{Bmatrix} \omega_r - i\frac{\kappa_r}{2} & 0 \\ 0 & \omega_m - i\frac{\kappa_m}{2} \end{Bmatrix} + \Sigma. \quad \text{(C5)}$$

[1] P. Warwick and J. Gerard, *Quantum Optomechanics* (CRC Press, Boca Raton, FL, 2016).
[2] M. Aspelmeyer, T. Kippenberg, and F. Marquardt, Rev. Mod. Phys. **86**, 1391 (2014).
[3] T. Kippenberg and K. Vahala, Opt. Express **15**, 17172 (2007).
[4] B. Peng, Ş. K. Özdemir, W. Chen, F. Nori, and L. Yang, Nat. Commun. **5**, 5082 (2014).
[5] G. Anetsberger, O. Arcizet, Q. P. Unterreithmeier, R. Rivière, A. Schliesser, E. M. Weig, J. P. Kotthaus, and T. J. Kippenberg, Nat. Phys. **5**, 909 (2009).
[6] T. Kippenberg and K. Vahala, Science **321**, 1172 (2008).
[7] J. T. Hill, A. H. Safavi-Naeini, J. Chan, and O. Painter, Nat. Commun. **3**, 1196 (2012).
[8] Y.-C. Liu, Y.-F. Xiao, X. Luan, and C. W. Wong, Phys. Rev. Lett. **110**, 153606 (2013).
[9] T. Corbitt, Y. Chen, E. Innerhofer, H. Müller-Ebhardt, D. Ottaway, H. Rehbein, D. Sigg, S. Whitcomb, C. Wipf, and N. Mavalvala, Phys. Rev. Lett. **98**, 150802 (2007).
[10] J. D. Thompson, B. M. Zwickl, A. M. Jayich, F. Marquardt, S. M. Girvin, and J. G. E. Harris, Nature (London) **452**, 72 (2008).
[11] X. Zhang, C.-L. Zou, L. Jiang, and H. X. Tang, Phys. Rev. Lett. **113**, 156401 (2014).
[12] T. Liu, X. Zhang, H. X. Tang, and M. E. Flatté, Phys. Rev. B **94**, 060405 (2016).
[13] X. Zhang, N. Zhu, C.-L. Zou, and H. X. Tang, Phys. Rev. Lett. **117**, 123605 (2016).
[14] J. A. Haigh, S. Langenfeld, N. J. Lambert, J. J. Baumberg, A. J. Ramsay, A. Nunnenkamp, and A. J. Ferguson, Phys. Rev. A **92**, 063845 (2015).
[15] J. Bourhill, N. Kostylev, M. Goryachev, D. L. Creedon, and M. E. Tobar, Phys. Rev. B **93**, 144420 (2016).
[16] A. Osada, R. Hisatomi, A. Noguchi, Y. Tabuchi, R. Yamazaki, K. Usami, M. Sadgrove, R. Yalla, M. Nomura, and Y. Nakamura, Phys. Rev. Lett. **116**, 223601 (2016).
[17] J. A. Haigh, A. Nunnenkamp, A. J. Ramsay, and A. J. Ferguson, Phys. Rev. Lett. **117**, 133602 (2016).
[18] S. V. Kusminskiy, H. X. Tang, and F. Marquardt, Phys. Rev. A **94**, 033821 (2016).
[19] J. W. Kłos, M. Krawczyk, Y. S. Dadoenkova, N. Dadoenkova, and I. Lyubchanskii, J. Appl. Phys. **115**, 174311 (2014).
[20] A. Chumak, V. Vasyuchka, A. Serga, and B. Hillebrands, Nat. Phys. **11**, 453 (2015).
[21] Y. Tabuchi, S. Ishino, A. Noguchi, T. Ishikawa, R. Yamazaki, K. Usami, and Y. Nakamura, Science **349**, 405 (2015).
[22] H. Huebl, C. W. Zollitsch, J. Lotze, F. Hocke, M. Greifenstein, A. Marx, R. Gross, and S. T. B. Goennenwein, Phys. Rev. Lett. **111**, 127003 (2013).
[23] D. W. Brooks, T. Botter, S. Schreppler, T. P. Purdy, N. Brahms, and D. M. Stamper-Kurn, Nature (London) **488**, 476 (2012).
[24] A. H. Safavi-Naeini, S. Gröblacher, J. T. Hill, J. Chan, M. Aspelmeyer, and O. Painter, Nature (London) **500**, 185 (2013).
[25] T. P. Purdy, P.-L. Yu, R. W. Peterson, N. S. Kampel, and C. A. Regal, Phys. Rev. X **3**, 031012 (2013).
[26] J.-Q. Liao and C. K. Law, Phys. Rev. A **83**, 033820 (2011).
[27] A. Nunnenkamp, K. Børkje, J. G. E. Harris, and S. M. Girvin, Phys. Rev. A **82**, 021806 (2010).
[28] O. Arcizet, P.-F. Cohadon, T. Briant, M. Pinard, A. Heidmann, J.-M. Mackowski, C. Michel, L. Pinard, O. Français, and L. Rousseau, Phys. Rev. Lett. **97**, 133601 (2006).
[29] M. Tsang and C. M. Caves, Phys. Rev. Lett. **105**, 123601 (2010).
[30] J. Teufel, T. Donner, M. Castellanos-Beltran, J. Harlow, and K. Lehnert, Nat. Nanotechnol. **4**, 820 (2009).
[31] S. Nimmrichter, K. Hornberger, and K. Hammerer, Phys. Rev. Lett. **113**, 020405 (2014).
[32] A. B. Shkarin, N. E. Flowers-Jacobs, S. W. Hoch, A. D. Kashkanova, C. Deutsch, J. Reichel, and J. G. E. Harris, Phys. Rev. Lett. **112**, 013602 (2014).
[33] S. Weis, R. Rivière, S. Deléglise, E. Gavartin, O. Arcizet, A. Schliesser, and T. J. Kippenberg, Science **330**, 1520 (2010).
[34] F. Monifi, J. Zhang, Ş. K. Özdemir, B. Peng, Y.-x. Liu, F. Bo, F. Nori, and L. Yang, Nat. Photonics **10**, 399 (2016).
[35] A. H. Safavi-Naeini, T. M. Alegre, J. Chan, M. Eichenfield, M. Winger, Q. Lin, J. T. Hill, D. E. Chang, and O. Painter, Nature (London) **472**, 69 (2011).
[36] H. Jing, Ş. K. Özdemir, Z. Geng, J. Zhang, X.-Y. Lü, B. Peng, L. Yang, and F. Nori, Sci. Rep. **5**, 9663 (2015).
[37] K. Stannigel, P. Komar, S. J. M. Habraken, S. D. Bennett, M. D. Lukin, P. Zoller, and P. Rabl, Phys. Rev. Lett. **109**, 013603 (2012).
[38] Y.-D. Wang and A. A. Clerk, New J. Phys. **14**, 105010 (2012).
[39] Y.-C. Liu, Y.-F. Xiao, Y.-L. Chen, X.-C. Yu, and Q. Gong, Phys. Rev. Lett. **111**, 083601 (2013).

[40] M. Ludwig, A. H. Safavi-Naeini, O. Painter, and F. Marquardt, Phys. Rev. Lett. **109**, 063601 (2012).
[41] A. A. Serga, A. V. Chumak, and B. Hillebrands, J. Phys. D **43**, 264002 (2010).
[42] M. Montagnese, M. Otter, X. Zotos, D. A. Fishman, N. Hlubek, O. Mityashkin, C. Hess, R. Saint-Martin, S. Singh, A. Revcolevschi, and P. H. M. van Loosdrecht, Phys. Rev. Lett. **110**, 147206 (2013).
[43] B. Lenk, H. Ulrichs, F. Garbs, and M. Münzenberg, Phys. Rep. **507**, 107 (2011).
[44] R. P. Cowburn and M. E. Welland, Science **287**, 1466 (2000).
[45] A. Imre, G. Csaba, L. Ji, A. Orlov, G. H. Bernstein, and W. Porod, Science **311**, 205 (2006).
[46] H. Tanji, S. Ghosh, J. Simon, B. Bloom, and V. Vuletić, Phys. Rev. Lett. **103**, 043601 (2009).
[47] J. Lorenzana and G. A. Sawatzky, Phys. Rev. Lett. **74**, 1867 (1995).
[48] X. Zhang, C.-L. Zou, N. Zhu, F. Marquardt, L. Jiang, and H. X. Tang, Nat. Commun. **6**, 8914 (2015).
[49] S. Demokritov, B. Hillebrands, and A. Slavin, Phys. Rep. **348**, 441 (2001).
[50] P. A. Fleury and R. Loudon, Phys. Rev. **166**, 514 (1968).
[51] D. Armani, T. Kippenberg, S. Spillane, and K. Vahala, Nature (London) **421**, 925 (2003).
[52] K. J. Vahala, Nature (London) **424**, 839 (2003).
[53] M. L. Gorodetsky and V. S. Ilchenko, J. Opt. Soc. Am. B **16**, 147 (1999).
[54] D. Lee, M. Underwood, D. Mason, A. B. Shkarin, S. W. Hoch, and J. G. E. Harris. Nat. Commun. **6**, 6232 (2015)..
[55] H. Xu, D. Mason, L. Jiang, and J. G. E. Harris, Nature (London) **537**, 80 (2016).
[56] H. Xu, D. Mason, L. Jiang, and J. G. E. Harris, arXiv:1703.07374 (2017).
[57] T. Kushida, *Magneto-optics*, Springer Series in Solid-State Sciences Vol. 128 (Springer, Berlin, 2000).
[58] H. S. Bennett and E. A. Stern, Phys. Rev. **137**, A448 (1965).
[59] M. Inoue and T. Fujii, J. Appl. Phys. **81**, 5659 (1997).
[60] A. Kirilyuk, A. V. Kimel, and T. Rasing, Rev. Mod. Phys. **82**, 2731 (2010).
[61] A. Kimel, A. Kirilyuk, P. Usachev, R. Pisarev, A. Balbashov, and T. Rasing, Nature (London) **435**, 655 (2005).
[62] M. Gorodetsky and V. Ilchenko, Opt. Commun. **113**, 133 (1994).
[63] J. M. Taylor, A. S. Sørensen, C. M. Marcus, and E. S. Polzik, Phys. Rev. Lett. **107**, 273601 (2011).
[64] A. Ashkin, *Optical Trapping and Manipulation of Neutral Particles Using Lasers: A Reprint Volume with Commentaries* (World Scientific, Singapore, 2006).